

Landslides (2017) 14:1389–1401

DOI 10.1007/s10346-016-0783-6

Received: 26 July 2016

Accepted: 20 November 2016

Published online: 16 December 2016

© The Author(s) 2016

This article is published with open access at Springerlink.com

Carolina de Lima Neves Seefelder · Sérgio Koide · Martin Mergili

Does parameterization influence the performance of slope stability model results? A case study in Rio de Janeiro, Brazil

Abstract We produce factor of safety (*FOS*) and slope failure susceptibility index (*SFSI*) maps for a 4.4-km² study area in Rio de Janeiro, Brazil, in order to explore the sensitivity of the geotechnical and geohydraulic parameterization on the model outcomes. Thereby, we consider parameter spaces instead of combinations of discrete values. *SFSI* is defined as the fraction of tested parameter combinations within a given space yielding *FOS* < 1. We repeat our physically based calculations for various parameter spaces, employing the infinite slope stability model and the sliding surface model of the software *r.slope.stability* for testing the geotechnical parameters and the Transient Rainfall Infiltration and Grid-Based Regional Slope-Stability Model (*TRIGRS*) for testing the geohydraulic parameters. Whilst the results vary considerably in terms of their conservativeness, the ability to reproduce the spatial patterns of the observed landslide release areas is relatively insensitive to the variation of the parameterization as long as there is sufficient pattern in the results. We conclude that landslide susceptibility maps yielded by catchment-scale physically based models should not be interpreted in absolute terms and suggest that efforts to develop better strategies for dealing with the uncertainties in the spatial variation of the key parameters should be given priority in future slope stability modelling efforts.

Keywords Parameter sensitivity · Parameter space · Slope failure susceptibility index · Slope stability model · *TRIGRS* · Uncertainty

Introduction

Landslides starting from unstable slopes affect the safety of life as well as of private and public assets. Computer models are employed to identify potentially unstable areas in order to facilitate decision-making at various levels. Whilst statistical models explore the relationships between the spatial patterns of landslide occurrence and a set of predictor layers, physically based models attempt to reproduce or to predict the physical mechanisms involved (Guzzetti et al. 1999; Van Westen 2000; Guzzetti 2006; Van Westen et al. 2006). Physically based models are frequently employed to estimate landslide susceptibility at the scale of small catchments (Van Westen et al. 2006). As long as shallow landslides are considered, these approaches mostly rely on the infinite slope stability model. It is commonly used in raster-based geographic information system (GIS) environments to derive a factor of safety for each pixel. However, the infinite slope stability model is unconditionally suitable only for those areas where shallow translational landslides with a length-to-depth ratio $L/D > 16$ –25 are expected (Griffiths et al. 2011; Milledge et al. 2012). As shallow landslides are most commonly triggered by extreme hydrometeorological events, such modelling tools are often coupled with more or less complex hydraulic models (e.g., Montgomery and Dietrich 1994; Van Westen and Terlien 1996; Burton and Bathurst 1998; Pack

et al. 1998; Wilkinson et al. 2002; Xie et al. 2004a; Baum et al. 2008; Godt et al. 2008; Muntohar and Liao 2010; Mergili et al. 2012).

For areas with deep-seated landslides, models assuming spherical, ellipsoidal or complex sliding surfaces reproduce the stability situation in a more appropriate way. Whilst they are standard in geotechnical engineering, their implementation with GIS is non-trivial so that catchment-scale applications are less commonly applied (e.g. Xie et al. 2003, 2004b, 2006; Jia et al. 2012; Mergili et al. 2014a, b).

Even simple slope stability or hydraulic models rely on parameters which are highly uncertain in their horizontal and vertical distribution. One possible concept to account for parameter uncertainty is the probability of failure (Tobutt 1982) which has started to complement the conventional factor of safety with increasing computational power, considering parameter spaces using random or regular sampling of uncertain parameters (Mergili et al. 2014a). Various authors have introduced and used different types of probability density functions (pdfs) of geotechnical (El-Ramly et al. 2005; Petrovic 2008; Mergili et al. 2014a) and geohydraulic parameters (Mesquita et al. 2002, 2007; Mesquita and Moraes 2004) which can be employed for parameter sampling. Whilst such functions are a smart way to deal with uncertain information, they are not necessarily transferable between different locations and therefore commonly suffer from small sample sizes and, consequently, weakly supported means and standard deviations.

As the challenge of uncertain parameters is encountered in many fields of geosciences, various approaches have been developed in the previous decades to test the sensitivity of the model results or the model performance to the input parameters or to optimize (calibrate) the input parameters in order to bring the model results in line with reference observations. Testing one parameter at a time is thereby considered inappropriate as both the optimum value and the sensitivity may strongly interrelate with the values of other parameters (Saltelli and Annoni 2010). Multi-parameter strategies are therefore required (e.g., Duan et al. 1992; Eberhart and Kennedy 1995; Hay et al. 2006; Vrugt et al. 2008; Fischer 2013). Optimized parameters or parameter sets, however, are not necessarily meaningful from a physical point of view. Particularly when calibrating many parameters at once, a good model performance in terms of reproducing the observation can be achieved despite a poor process understanding. The sensitivity of local-scale slope stability model results to selected input parameters was tested, e.g. by Griffiths and Fenton (2004) or by Wang et al. (2010). Guimarães et al. (2003) and Formetta et al. (2015) have applied parameter optimization strategies at catchment scale.

Almost all documented parameter sensitivity and optimization strategies target at discrete parameter values. We think that, particularly at broader scales, sensitivity analysis and optimization of

parameter values is inappropriate as it disregards the inherent fine-scale spatial variability of the parameters. Instead, we suggest performing sensitivity analysis and optimization of parameter ranges.

The present article demonstrates such a strategy, employing a modification of the probability of failure concept. We investigate how the considered ranges of geotechnical and geohydraulic input parameters influence the results and performance of GIS-based catchment-scale slope stability models. For this purpose, we apply the infinite slope stability model, the sliding surface model of the tool *r.slope.stability* and the software Transient Rainfall Infiltration and Grid-Based Regional Slope-Stability Model (TRIGRS) to the Quitite and Papagaio catchments, Rio de Janeiro, Brazil. The findings are thought to be useful to identify suitable parameterization strategies for future slope stability modelling efforts.

Next, we introduce the study area (“Study area and data” section) and describe the components of the proposed work flow (“Methods” section). We then demonstrate (“Results” section) and discuss (“Discussion” section) the results obtained before drawing our conclusions (“Conclusions” section).

Study area and data

The study area includes the two landslide-prone Quitite and Papagaio watersheds located in the western part of the city of Rio de Janeiro, Brazil (Fig. 1). Together, they cover an area of

4.4 km², extending between 12 and 995 m a.s.l. The climate in the area is tropical humid (Guimarães et al. 2009). Due to influence by ocean moisture, the area receives a higher amount of rainfall than the central part of Rio de Janeiro (Hurtado Espinoza 2010). Granitic bedrock dominates both watersheds. The homogeneous, colluvial yellow soil is characterized by sandy-clay features (Hurtado Espinoza 2010; Galindo 2013; Galindo and Campos 2014) and a depth of 1–3 m (Guimarães et al. 2003). Native forest is still the dominant type of vegetation whilst the anthropogenic influence on the land cover is of limited importance (Guimarães et al. 2003; Hurtado Espinoza 2010).

Guimarães et al. (2003) optimized values of effective cohesion c' (kN m⁻²), normalized to depth d , effective angle of internal friction ϕ' and specific weight of the saturated soil γ_s (kN m⁻³) using published parameters for geomorphologically comparable adjacent areas and back-calculations with the software SHALSTAB. These authors arrived at best fit values of $c'/d = 2$ kN m⁻³, $\phi' = 45^\circ$ and $\gamma_s = 15$ kN m⁻³, but they also indicated that, in general, low values of c'/d , high values of ϕ' and values from 15 to 17.5 kN m⁻³ for γ_s would be appropriate for the area. They proposed a general frame of parameter values realistic for the area (in the sense of a parameter space) summarized in Table 1 and, with some modifications, applied to tests A and B (see “Methods” and “Results” sections). Hurtado Espinoza (2010) measured a dry specific weight around 15 kN m⁻³ for some undisturbed samples taken at

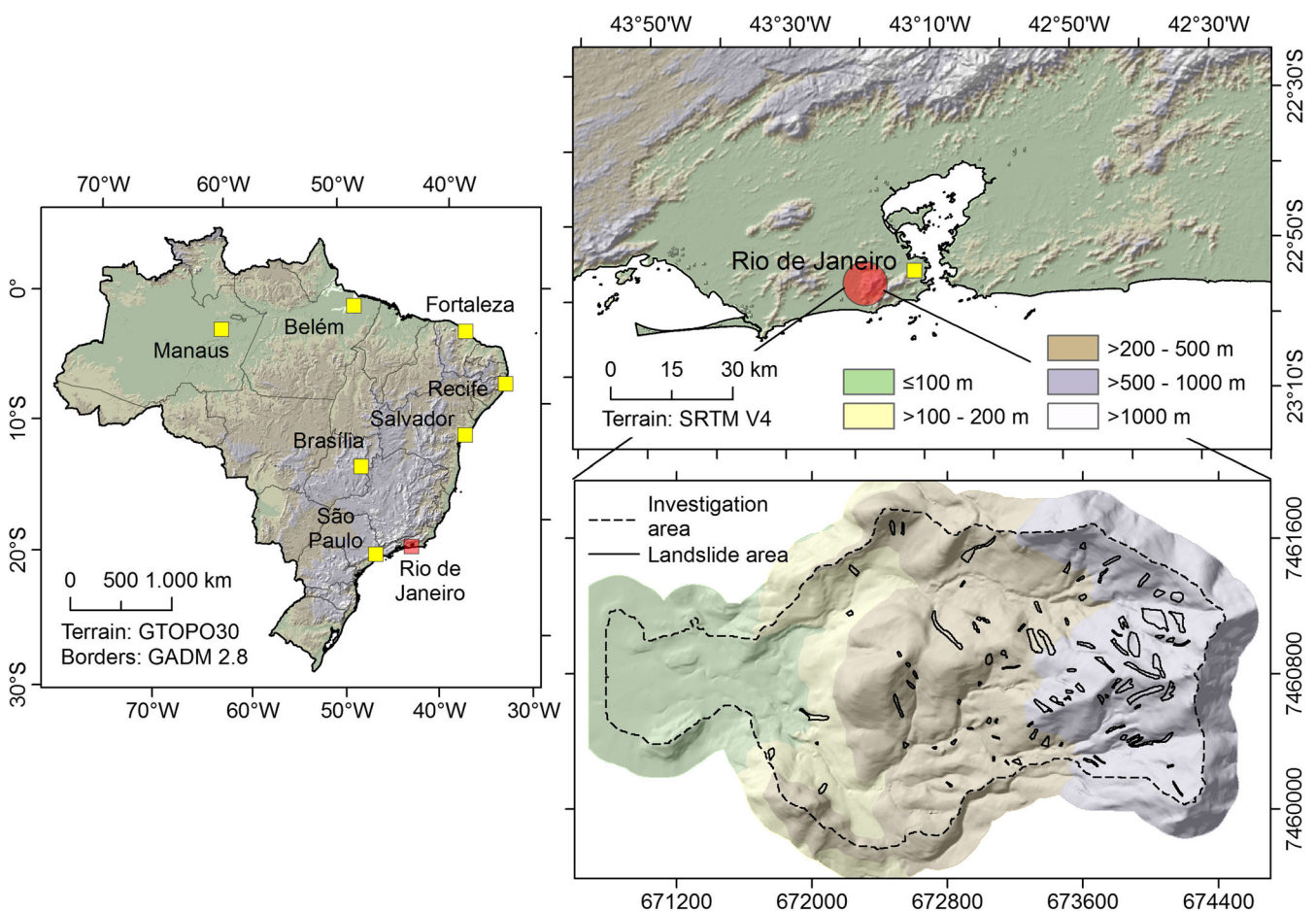


Fig. 1. The study area, consisting in the two catchments Quitite and Papagaio in Rio de Janeiro, Brazil

Table 1 Range of parameter values applicable to the Quitite and Papagaio watersheds (Guimarães et al. 2003)

Parameter	Minimum value	Maximum value
c'/d	0 kPa m ⁻¹	8 kPa m ⁻¹
ϕ'	25°	45°
γ_s	15,000	25,000

1 m depth. The same authors stated that the slopes in the lower areas would be weaker whilst those in the higher areas would be stronger.

Values of soil saturated conductivity K_s were measured by Fernandes et al. (2001) using Guelph's permeameter. The results showed a high variability with values ranging from 10^{-6} to 10^{-4} m s⁻¹ as well as some important discontinuities in the profiles, possibly influencing groundwater flow.

We consider a landslide event related to intense rainfall on 13 and 14 February 1996. Within 48 h, 394.3 mm of rainfall was registered at the Alto da Boa Vista station, and 245.9 mm at the Jacarepaguá station, both located in close vicinity to the Quitite and Papagaio catchments and operated by the National Meteorological Institute (INMET; Conti 2012). A landslide inventory developed by Guimarães (2000) is used in the present work. According to this inventory, the rainfall event has triggered 93 landslides, occupying 0.14 km² (3.1% of the entire area). Table 2 summarizes the main characteristics of the landslide inventory. Most landslides occurred in the native forest areas dominating the study area. Shallow landslides, debris flows and debris avalanches were most common. The sliding surfaces of most landslides coincided with the soil-rock interface (Guimarães et al. 2003; Miqueletto and Vargas, 2009; Hurtado Espinoza 2010). The landslide inventory displays the entire extent of the directly affected areas without distinguishing between release, transit and deposition areas.

Besides the geotechnical and geohydraulic information and the landslide inventory, we use a 2-m resolution digital elevation model (DEM).

Methods

Work flow and software

Figure 2 illustrates the general work flow of the study. We compute the slope failure susceptibility index (*SFSI*) (dimensionless number in the range 0–1) based on sets of factor of safety (*FOS*) values derived through the controlled variation of selected key parameters within a defined parameter sub-space. This procedure is repeated for various sub-spaces. The resulting *SFSI* values are

evaluated against the inventory of observed landslides, and the findings are compared and interpreted.

In a first step, we vary the geotechnical parameters (tests A and B) and in a second step, we vary the geohydraulic parameters (test C). Test D uses a simple statistical model for the sake of comparison. Test A builds on the infinite slope stability model, test B on the sliding surface model of the tool *r.slope.stability* (Mergili et al. 2014a, b), designed as a raster module of the open source GRASS GIS software (Neteler and Mitasova 2008; GRASS Development Team 2016). Test C makes use of TRIGRS (Transient Rainfall Infiltration and Grid-Based Regional Slope-Stability Model; Baum et al. 2008), which is a grid-based tool simulating the permanent and transient rainfall influences on slope stability. Python scripting is used to derive *SFSI*, and the R Project for Statistical Computing (R Core Team, 2016) is employed for the evaluation of the results. Test D relies entirely on Python and R scripting.

Geotechnical model

Slope stability modelling commonly builds on the limit equilibrium theory (Duncan and Wright 2005): a factor of safety (*FOS*) is computed as the ratio between resisting forces *R* and driving forces *T*:

$$FOS = \frac{R}{T} \quad (1)$$

When *FOS* = 1, the slope is in static equilibrium. Values of *FOS* <1 indicate potential failure (in reality, such slopes do not exist), values of *FOS* >1 indicate stable slopes. The use of this method requires the prior definition of a slip surface, and the soil is considered as rigid material.

For GIS-supported catchment-scale analyses of slope stability, the infinite slope stability model is most commonly employed (Montgomery and Dietrich 1994; Pack et al. 1998; Xie et al. 2004a; Baum et al. 2008). It assumes (i) a uniform slope of infinite length, and (ii) a plane, slope-parallel failure surface. As inter-slice forces do not have to be considered, it is conveniently applied on a pixel-to-pixel basis. Based on Eq. (1), *FOS* can be expressed in various ways. For fully saturated soil, the equation may be formulated as follows (modified after Baum et al. 2008):

$$FOS = \frac{\tan\phi}{\tan\alpha} + \frac{c - u \tan\phi}{\gamma_s d \sin\alpha \cos\alpha} \quad (2)$$

where α is the slope angle, *u* (N m⁻²) is the pore water pressure, γ_s (N m⁻³) is the specific weight of the saturated soil and *d* (m) is the depth of the sliding surface.

Table 2 Main characteristics of the inventoried landslides triggered by the rainfall event of 13 and 14 February 1996 in the Quitite and Papagaio watersheds

Landslide characteristics	Values
Number of landslides	93
Total landslide area (fraction of total area)	0.14 km ² (3.1%)
Average (minimum–maximum) landslide area projected to ground plot	1520 m ² (32–11,904)
Average (minimum–maximum) landslide length in down-slope direction, projected to ground plot	65.9 m (8.0–220.0)
Average (minimum–maximum) landslide width in cross-slope direction	20.0 m (4.0–96.0)
Average (minimum–maximum) landslide inclination in down-slope direction	31.9 (8.5–45.8)°

In the present work, we use the infinite slope stability model implemented with *r.slope.stability* and with TRIGRS. Alternatively, we also apply the sliding surface model of *r.slope.stability*. Thereby, the slope stability is tested for a large number of randomly selected ellipsoid-shaped potential sliding surfaces, truncated at the depth of the soil. R and T are summarized over all pixels intersecting a given sliding surface, and FOS is computed for each surface in a way analogous to Eqs. 1 and 2, applying a modification of the Hovland (1977) model. Finally, the minimum value of FOS resulting from the overlay of all sliding surfaces is applied to each pixel. For a more detailed description of the sliding surface model of *r.slope.stability*, we refer to Mergili et al. (2014a, b).

Geohydraulic model

In TRIGRS, FOS is computed for one or more user-defined depths. The Richard's equation is used to calculate the soil transient infiltration for saturated and unsaturated soil conditions (Iverson 2000):

$$\frac{\partial \psi}{\partial t} \frac{d\theta}{d\psi} = \frac{\partial}{\partial x} \left[K_L(\psi) \left(\frac{\partial \psi}{\partial x} - \sin \alpha \right) \right] + \frac{\partial}{\partial y} \left[K_L(\psi) \left(\frac{\partial \psi}{\partial y} \right) \right] + \frac{\partial}{\partial z} \left[K_z(\psi) \left(\frac{\partial \psi}{\partial z} - \cos \alpha \right) \right] \quad (3)$$

where ψ (m) is pressure head, θ is soil volumetric water content, t (s) is time, K_L (m s^{-1}) is lateral soil conductivity and K_z (m s^{-1}) is soil conductivity in z direction.

To solve the Richards equation, TRIGRS uses an approach developed by Iverson (2000), considering homogeneous soil, isotropic flow, relatively shallow depth, one-dimensional vertical downslope flow and soil moisture close to saturated conditions (Baum et al. 2008; Park et al. 2013), following the heat conduction approach described by Carslaw and Jaeger (1959). We refer to Baum et al. (2008) for a detailed description of the procedure.

For computing the groundwater level, TRIGRS compares the infiltrated water volume V_i and the maximum drainage capacity of the soil V_D . If $V_D \geq V_i$, the water table remains constant. Otherwise, the water table rises, depending on K_s and the transmissivity T . For unsaturated conditions, the maximum value of ψ is the new water level multiplied with β (value set according to the adopted flow condition). The amount of water exceeding the maximum infiltration rate is considered surficial runoff. However, surficial runoff is not taken over from one time step to the next (Baum et al. 2008).

Slope failure susceptibility index

The slope failure susceptibility index ($SFSI$) in the range 0–1 refers to the fraction of geotechnical and/or geohydraulic parameter combinations resulting in $FOS < 1$, out of an arbitrary number of tested parameter combinations. This means that $SFSI$ for a given pixel increases with each parameter combination where $FOS < 1$ and, finally, low values of FOS correspond to high values of $SFSI$. The principal concept of the $SFSI$ is identical to the concept of the slope failure probability yielded by *r.slope.stability* (Mergili et al. 2014a). However, we refer to it as a susceptibility index in the context of the present study as we simply use a uniform probability density function throughout all the computations. Such a distribution does not necessarily capture the real-world parameter distribution (which is unknown) and its use does therefore not justify applying the concept of probability in a strict sense.

Statistical model

In test D, a statistical model is applied for the purpose of comparison, employing the slope angle as the only predictor layer (Table 3). We keep the statistical model as basic as possible in order to evaluate the performance of a simplistic statistical approach in comparison to the physically based models (“Geotechnical model” to “Slope failure susceptibility index” sections). This allows us to conclude on the need of using more complex physically based models for catchment-scale landslide susceptibility analysis. Thereby, we overlay a classified slope map with the map of the observed landslide release areas (ORA; “Model evaluation” section) and, for each slope class, compute the fraction f_C of observed landslide release pixels related to all pixels. $SFSI$ —referred to as release probability by Mergili and Chu (2015) who employed a comparable approach—is then computed by applying f_C to all pixels of the corresponding slope class. Thereby, it is important to use two different areas for the derivation of f_C and for the computation and evaluation of $SFSI$ (“Test layout” section).

Model evaluation

The landslide inventory for the Quitite and Papagaio watersheds displays the entire observed landslide impact areas (OIAs), i.e. the release, transit and deposition areas without any differentiation. We approximate the ORA as the upper third part of each OIA polygon. Depending on the test (“Test layout” section and Table 3), either the OIA map or the ORA map is overlaid with the corresponding $SFSI$ map. When using the ORA map, the lower two-

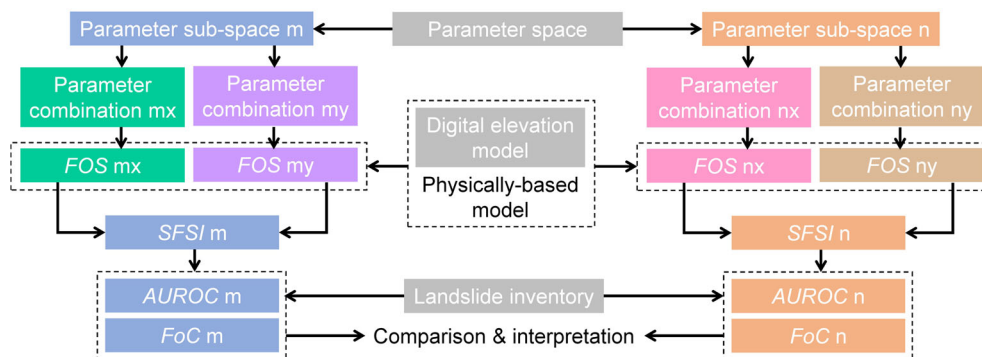


Fig. 2. Work flow of the study

thirds portion of the OIA is not considered for evaluation. The true positive (TP), true negative (TN), false positive (FP) and false negative (FN) pixel counts are derived for selected levels of *SFSI*. An ROC curve is produced by plotting the true positive rates TP/(TP + FN) against the false positive rates FP/(FP + TN) derived with each combination of parameters. The area under the ROC curve *AUROC* indicates the predictive capacity of the model: *AUROC* = 1.0 (the maximum) means a perfect prediction, *AUROC* = 0.5 (corresponding to a straight diagonal line) indicates a random prediction, i.e. model failure. *AUROC* refers to the entire area used for model evaluation.

In addition, we introduce a conservativeness measure:

$$\text{FoC} = \frac{\mu_{\text{SFSI}}}{r_{\text{OP}}} \quad (4)$$

where μ_{SFSI} is the average of *SFSI* over the entire study area, and r_{OP} is the observed positive rate, i.e. the fraction of observed landslide pixels out of all pixels in the study area. If $\text{FoC} > 1$, the model overestimates the landslide susceptibility, compared to the observation whilst values $\text{FoC} < 1$ indicate an underestimation of the landslide susceptibility.

Test layout

Tables 3 and 4 summarize the main characteristics of each test and the parameter values and ranges considered.

In a first step (tests A1–A4 and B), the sensitivity of *SFSI* and the associated model performance to the geotechnical parameters c' and ϕ' and the shape of the sliding surface is explored, assuming fully water-saturated soils, and the depth of the sliding surface corresponding with the soil depth. The infinite slope stability model and the sliding surface model implemented in *r.slope.stability* are employed for this purpose. We introduce a two-dimensional parameter space constrained by lower boundaries of $c' = 0 \text{ kN m}^{-3}$ and $\phi' = 21^\circ$, and upper boundaries of c'

$= 24 \text{ kN m}^{-3}$ and $\phi' = 45^\circ$ (Fig. 3a; Table 4). This parameter space accounts for the full ranges of c' and ϕ' considered representative for the area (“Study area and data” section). We note that the resulting values of *FOS* vary according to ϕ' and c'/d , so that the value of *FOS* obtained with $d = 3 \text{ m}$ and with a given value of c' is identical (infinite slope stability model) or similar (sliding surface model) to the value of *FOS* with other values of c' and d , but the same c'/d ratio. The dry specific weight of the soil $\gamma_d = 13.5 \text{ kN m}^{-2}$ and the volumetric saturated water content $\theta_s = 40 \text{ vol.}\%$ are set to constant values. We neglect the weight of the trees and the effects of their root systems on the cohesion: sliding surfaces are assumed to develop beneath the rooting depth.

The ranges of both c' and ϕ' are (i) considered in their entire extent; (ii) subdivided into two sub-ranges of equal extent and (iii) subdivided into three sub-ranges of equal extent (Fig. 4a, b). Considering all possible combinations of sub-ranges of the two parameters results in 36 partly overlapping parameter sub-spaces with 25 corner points. *SFSI* is computed for each parameter sub-space, with ten sampled parameters in each dimension (Fig. 4c). This procedure may be extended to three or more dimensions or repeated at a finer level by employing the sub-space with the best model performance as the entire space for the next level. For reasons to be explained in the “Results” section, only one level is applied in the present work. This work flow is repeated for two assumptions of soil depth and two versions of the landslide inventory used for evaluation, resulting in a total of four sub-tests (Table 3).

Test C explores the sensitivity of *SFSI* and the associated model performance to K_s and the initial depth of the water table d_i (m). We introduce a two-dimensional parameter space constrained by lower boundaries of $K_s = 10^{-7} \text{ m s}^{-1}$ and $d_i = 0 \text{ m}$ and upper boundaries of $K_s = 10^{-4} \text{ m s}^{-1}$ and $d_i = 3 \text{ m}$ (Fig. 3b; Table 4). The ranges of values used are based on works of Saxton and Rawls (2006) and Guimarães et al. (2003). We set $\gamma_s = 16 \text{ kN m}^{-2}$, $\theta_s = 40 \text{ vol.}\%$, $\theta_r = 5 \text{ vol.}\%$, c

Table 3 Summary of all tests performed

Test	Description
A1	The infinite slope stability model is applied with a constant soil depth $d = 3 \text{ m}$; the entire OIA is considered for evaluation. This means that all observed landslide pixels are considered OP whilst all observed non-landslide pixels are considered ON.
A2	Infinite slope stability model, constant soil depth $d = 3 \text{ m}$; only the ORA is considered for evaluation: the pixels in the upper third of each observed landslide are considered OP, all other observed landslide pixels are considered no data; all observed non-landslide pixels are considered ON. This procedure helps to exclude pixels possibly representing transit or deposition areas from the evaluation procedure.
A3	Infinite slope stability model, variable soil depth and OIA considered for evaluation. According to Guimarães et al. (2003), d is varied between 1 and 3 m. We assume a linear increase of d within a certain range of the topographic wetness index (Moore et al. 1991).
A4	Infinite slope stability model, variable soil depth and ORA considered for evaluation
B	The sliding surface model implemented in <i>r.slope.stability</i> is applied along with the optimized parameters derived from the tests A1–A4. The ellipsoid density per pixel (Mergili et al. 2014a, b) is set to 2500. The ellipsoid dimensions are constrained by the dimensions of the release areas of the observed landslides. All ellipsoids are truncated at the depth of the soil.
C1	TRIGRS, rectangular hydrograph and an assumed rainfall duration of 6 h. The rainfall is considered constant throughout the entire period, resulting in an intensity of 24 mm/h.
C2	TRIGRS, rectangular hydrograph and rainfall duration of 10 h (intensity 14.4 mm/h)
C3	TRIGRS, triangular hydrograph with central peak and rainfall duration of 6 h, resulting in a peak intensity of 48 mm/h
C4	TRIGRS, triangular hydrograph with central peak and duration of 10 h and peak intensity of 28.8 mm/h
D	Simple statistical model employing the slope angle as the only predictor layer. Overlay of a classified slope map with the ORA map and, for each class, computation of the fraction of observed landslide release pixels related to all pixels.

For more details such as the parameters spaces applied please refer to the text

Table 4 Geotechnical and geohydraulic parameter values and ranges applied for the tests A–C (Table 3), following Guimarães et al. (2003); Saxton and Rawls (2006); Hurtado Espinoza (2010); Conti (2012); Park et al. (2013)

Symbol	Description	A1–A4	B	C1–C4
ϕ'	Effective angle of internal friction	21–45°	21–45°	45°
c'	Effective cohesion	0–24 kN m ⁻²	0–24 kN m ⁻²	4.5 kN m ⁻²
γ_d	Dry specific weight	13.5 kN m ⁻³	13.5 kN m ⁻³	N/A
γ_s	Saturated specific weight	N/A	N/A	16.0 kN m ⁻³
θ_s	Saturated water content	40 Vol.%	40 Vol.%	40 Vol.%
θ_r	Residual water content	N/A	N/A	5 Vol.%
K_s	Saturated hydraulic conductivity	N/A	N/A	10 ⁻⁷ –10 ⁻⁴ m s ⁻¹
D	Diffusivity	N/A	N/A	200 K_s
I_0	Initial infiltration rate	N/A	N/A	1.3 10 ⁻⁶ m s ⁻¹
d	Sliding surface depth	3 m	3 m ^a	3 m
d_w	Depth of water table	0 m	0 m	N/A
d_i	Initial depth of water table	N/A	N/A	0–3 m

^a In test B, the ellipsoid-shaped random slip surfaces are truncated at a depth of 3 m

' = 4.5 kN m⁻², $\phi' = 45^\circ$ and $d = 3$ m to constant values. The choice of these values is supported by data from Guimarães et al. (2003) and Hurtado Espinoza (2010). We further assume constant values of diffusivity ($D = 200K_s$; Park et al., 2013) and initial infiltration rate ($I_0 = 1.3 \cdot 10^{-6}$ m s⁻¹; Conti 2012).

In a way analogous to the geotechnical parameters, the ranges of both K_s and d_i are (i) considered in their entire extent, (ii) subdivided into two sub-ranges of equal extent and (iii) subdivided into three sub-ranges of equal extent, resulting in 36 partly overlapping parameter sub-spaces with 25 corner points. *SFSI* is computed for each parameter sub-space, with five sampled parameters in each dimension. The landslide inventory used for evaluation is ORA.

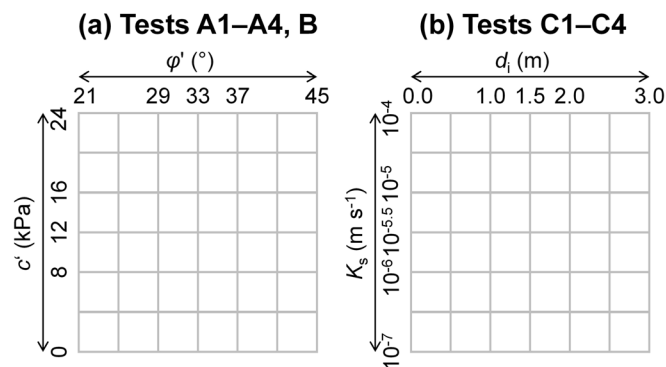
This procedure is repeated for four combinations of rainfall duration and type of pluviograph (Table 3). We assume rainfall durations of 6 and 10 h and a total rainfall amount derived from the measurements at the Jacarepaguá and Boa Vista stations on 13 and 14 February 1996 (Conti 2012). The Thiessen method is applied for estimating the precipitation in the catchment, and 20% of interception are deduced (Coelho Netto 2005). The total rainfall considered for the analysis is 144 mm in all the scenarios C1–C4.

In test D, we apply the statistical model introduced in the “Statistical model” section for the purpose of comparison (Table 3). f_c is derived for one of the two catchments. *SFSI* is then computed for the other catchment and evaluated against the corresponding ORA. The entire procedure is repeated in the reverse way, so that a clear separation between the model development and model evaluation areas is ensured.

Results

Tests A and B: geotechnical parameterization

Figure 5 illustrates the results of test A in terms of model performance (*AUROC*) and conservativeness (*FoC*). Assuming a constant soil depth, the model performs significantly better when considering only the ORA (test A2; $AUROC \leq 0.741$; Fig. 5b) instead of the entire OIA (test A1; $AUROC \leq 0.691$; Fig. 5a). This result clearly indicates that the OIA is unsuitable as reference for evaluation, and an appropriate inventory sub-setting is essential. Focusing on Fig. 5b, we note that the model performance in terms of *AUROC* is insensitive to the variation of the geotechnical parameterization within much of the tested ranges. In particular, the sub-

**Fig. 3.** Parameter spaces considered for the sensitivity analysis of the a geotechnical and b geohydraulic parameters

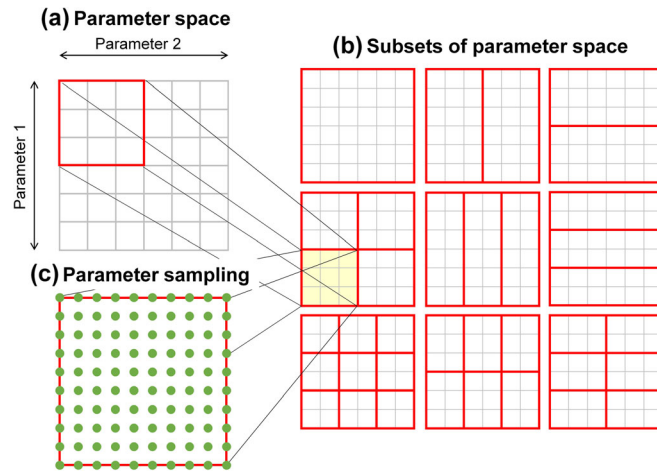


Fig. 4. Layout of the parameter sensitivity analysis procedure: **a** example of an arbitrary parameter space; **b** sub-setting of the parameter space into sub-spaces of various dimensions; **c** uniformly distributed parameter sampling within an arbitrary subspace. Each *dot* represents one parameter combination

spaces along a diagonal line from medium-high values of c' and low values of ϕ' to low values of c' and high values of ϕ' display almost identical *AUROC* values to the entire parameter space and to those sub-spaces including broad ranges of c' or broad ranges of ϕ' with medium-low values of c' . Only those sub-ranges limited to high values of c' or low values of c' and ϕ' yield significantly lower *AUROC* values. These sub-ranges result in poorly patterned relatively non-conservative and extremely conservative predictions, i.e. they display very low and very high *FoC* values, respectively. In general, the model results are very conservative, indicated by $FoC > 1$. At a lower level of *AUROC*—and a lower level of *FoC* caused by a higher number of OP pixels—similar patterns are observed in Fig. 5a.

Varying d as a function of the topographic wetness index exerts contrasting effects on the patterns of *AUROC*, depending on whether the OIA or the ORA is used as reference. With the ORA as reference (Test A4; Fig. 5d), the sub-spaces with low values of c' perform comparable to test A2 (Fig. 5b). This is not surprising as the influence of d on *FOS* increases with c' (with $c' = 0$, d has no influence). However, *AUROC* and also *FoC* decrease significantly with increasing c' , resulting in a very poor performance associated to those sub-spaces with high c' , and a reduced performance associated to those sub-spaces with broad ranges of c' , compared to Fig. 5b. This trend clearly indicates that most ORA pixels spatially coincide with areas of relatively low topographic wetness index and therefore low values of d (Table 3) resulting in high values of *FOS* and low values of *SFSI* in cohesive soils.

The reverse effect occurs when using the entire OIA as reference (test A3; Fig. 5c): many pixels in the lower portions of the landslide polygons coincide with high values of the topographic wetness index. Consequently, d and the resulting values of *SFSI* are comparatively high for many of the OP pixels, resulting in an improved model performance, compared to the tests A1 – A3 ($AUROC \leq 0.742$; Fig. 5b). However, since most of the lower parts of the landslide polygons do most likely not represent release areas, the increased performance represents an artefact of inappropriate assumptions rather than an indicator for model success.

Considering the findings outlined, we identify test A2 as most representative. Even though the full parameter space yields an

insignificantly lower value of *AUROC* than do some of the sub-spaces, there is no basis to support the choice of a particular sub-space in this specific case. The parameter values used and optimized by Guimarães et al. (2003) are mostly located within the parameter sub-spaces with the higher values of *AUROC*, indicating a certain plausibility of the results (Fig. 5b). Figure 6a shows the spatial patterns of *SFSI* derived in the tests A1 and A2 with the full parameter space of c' and ϕ' . We note that the results of those tests are similar in terms of *SFSI*, as only the reference information for validation is varied. The same is true for the *SFSI* maps derived through the tests A3 and A4 (Fig. 6b).

The spatial patterns of *SFSI* derived with the sliding surface model of r.slope.stability (test B) are illustrated in Fig. 6c. Applying the full parameter space of c' and ϕ' along with constant soil depth and the ORA as reference, the associated value of *AUROC* is almost identical to the value yielded with the infinite slope stability model (0.735 vs. 0.734 in test A2). Thereby, the results yielded with the sliding surface model are more conservative: $FoC = 59.5$, compared to a value of 48.3 yielded with the infinite slope stability model (Fig. 5b).

Test C: geohydraulic parameterization

Figure 7 illustrates the performance (*AUROC*) and conservativeness (*FoC*) of the model results for the various parameter sub-spaces of K_s and d_i . Firstly, we note that the results are largely insensitive to the four assumptions of rainfall duration and hydrograph shape (C1–C4): the patterns yielded are identical for all four scenarios, even though the numbers vary slightly. Within each scenario, the model performance responds highly sensitive to variations of K_s and d_i : it peaks at $AUROC = 0.719$ – 0.724 for the upper sub-range of the hydraulic conductivity ($K_s = 10^{-5}$ – 10^{-4} m s^{-1}) and the lower sub-range of the initial depth of the water table ($d_i = 0$ – 1 m). However, the model performance drops only slightly when the full range of both parameters K_s and d_i is applied ($AUROC = 0.711$ – 0.712). Figure 8 presents the *SFSI* maps produced in test C1 with the full space of K_s and d_i . The *SFSI* maps resulting from tests C2, C3 and C4 are almost similar to the map resulting from test C1 and are therefore not shown.



Fig. 5 Results of tests A1–A4 in terms of model performance ($AUROC$) and factor of conservativeness (FoC , in *italic letters*). See Fig. 3 for the configuration of the parameter space

Constraining the model input to the lower ranges of hydraulic conductivity or to deeper initial water tables leads to a significant drop in the model performance. Considering $K_s \leq 10^{-5.5}$ leads to model failure ($AUROC = 0.494$), independently of the range applied for d_i and the rainfall scenario. In this case, $FoC = 3.9$ (blue font colour in Fig. 7). As expected, FoC is highest for the configurations with high K_s and shallow d_i and lowest for the configurations with low K_s and deep d_i . Its maximum coincides with the best model performance ($FoC = 48.0$ – 48.9).

These outcomes reflect the fact that, with $K_s \leq 10^{-5.5}$, too little water propagates through the soil to substantially influence slope stability. The effect is similar with higher values of K_s if the initial water table is too deep. A shallower initial water table and higher values of K_s facilitate increased values of u over broad parts of the study area and, consequently, lead to less stable slopes (Eq. 2) and higher values of FoC . Only combinations of high K_s and deep d_i lead to a sufficient signal to reproduce the observed landslide release patterns with a fair

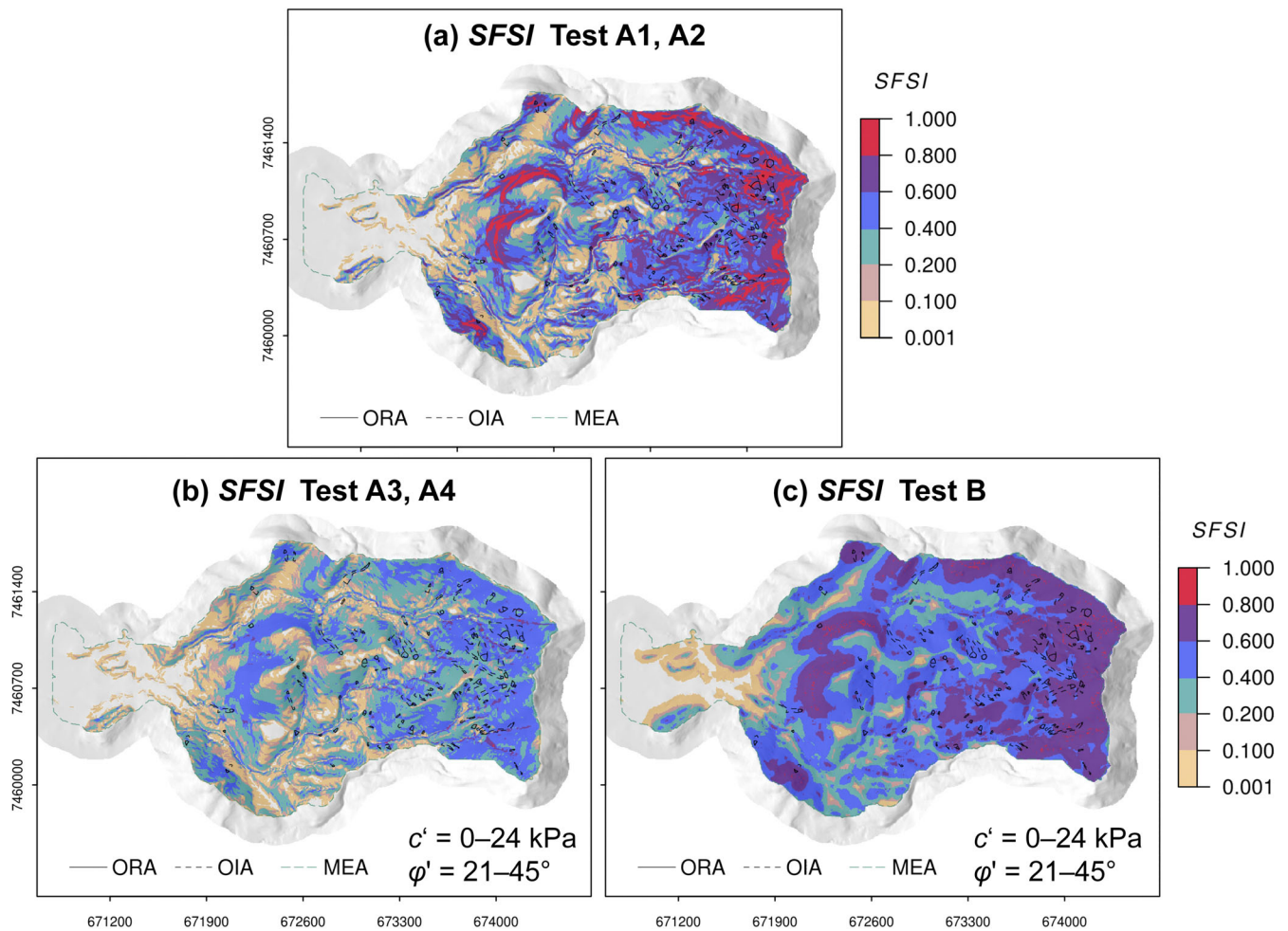


Fig. 6 SFSI maps resulting from the tests a A1 and A2; b A3 and A4 and c B, in each case relating to the full parameter space of c' and ϕ' . MEA model evaluation area

performance. As for tests A and B, all results are very conservative also for test C ($FoC > 1$).

Test D: statistical model

The statistical model yields an average AUROC value of 0.737 (values of 0.736 and 0.738 for the two catchments) whilst, as prescribed by the approach chosen, $FoC \approx 1$. The model performance corresponds remarkably well to the performance of the physically based models (tests A2 and B in particular), underlining the fact that the slope angle strongly dominates also the pattern of SFSI derived with the physically based models (Fig. 9).

Discussion

We have demonstrated that the performance of the physically based-derived slope failure susceptibility index SFSI in our study area reacts conditionally sensitive to variations in the considered spaces of selected geotechnical and geohydraulic input parameters and state variables. Those parameter configurations yielding insufficient pattern in terms of simulated landslide vs. non-landslide areas lead to a significantly poorer performance. With regard to the geotechnical information, comparable AUROC values are displayed throughout much of the parameter space considered relevant for the study area (Guimarães et al. 2003), except for

those sub-spaces with low c' and low ϕ' (μ_{SFSI} close to 1) and those areas with high c' and high ϕ' (μ_{SFSI} close to 0). This constellation underlines a well-known negative relationship between c' and ϕ' . Model performance in terms of AUROC responds very sensitive to variations in K_s and d_i within the tested ranges but insensitive to the variations in the rainfall scenarios applied. Whilst the findings for the geotechnical parameters are claimed to be broadly valid, those for K_s and d_i may strongly depend on the assumed rainfall duration and intensity in relation to the water capacity of the soil. In this sense, the pattern displayed in Fig. 7 might change for different rainfall events.

Our findings suggest that any further parameter optimization efforts in terms of AUROC may be obsolete: the pattern of SFSI derived with the entire parameter space performs approximately as well in reproducing the observed landslide areas as the patterns of SFSI derived with various sub-spaces do. Applying broad ranges of the key parameters for physically based catchment-scale landslide susceptibility modelling is on the “safe” side as it yields results comparable in quality to those derived with the best-fit narrower ranges. Acknowledging the fact that geotechnical and geohydraulic parameters are spatially highly variable, uncertain and often poorly known, applying a narrow parameter space—or even a singular combination of parameters—bears a considerable

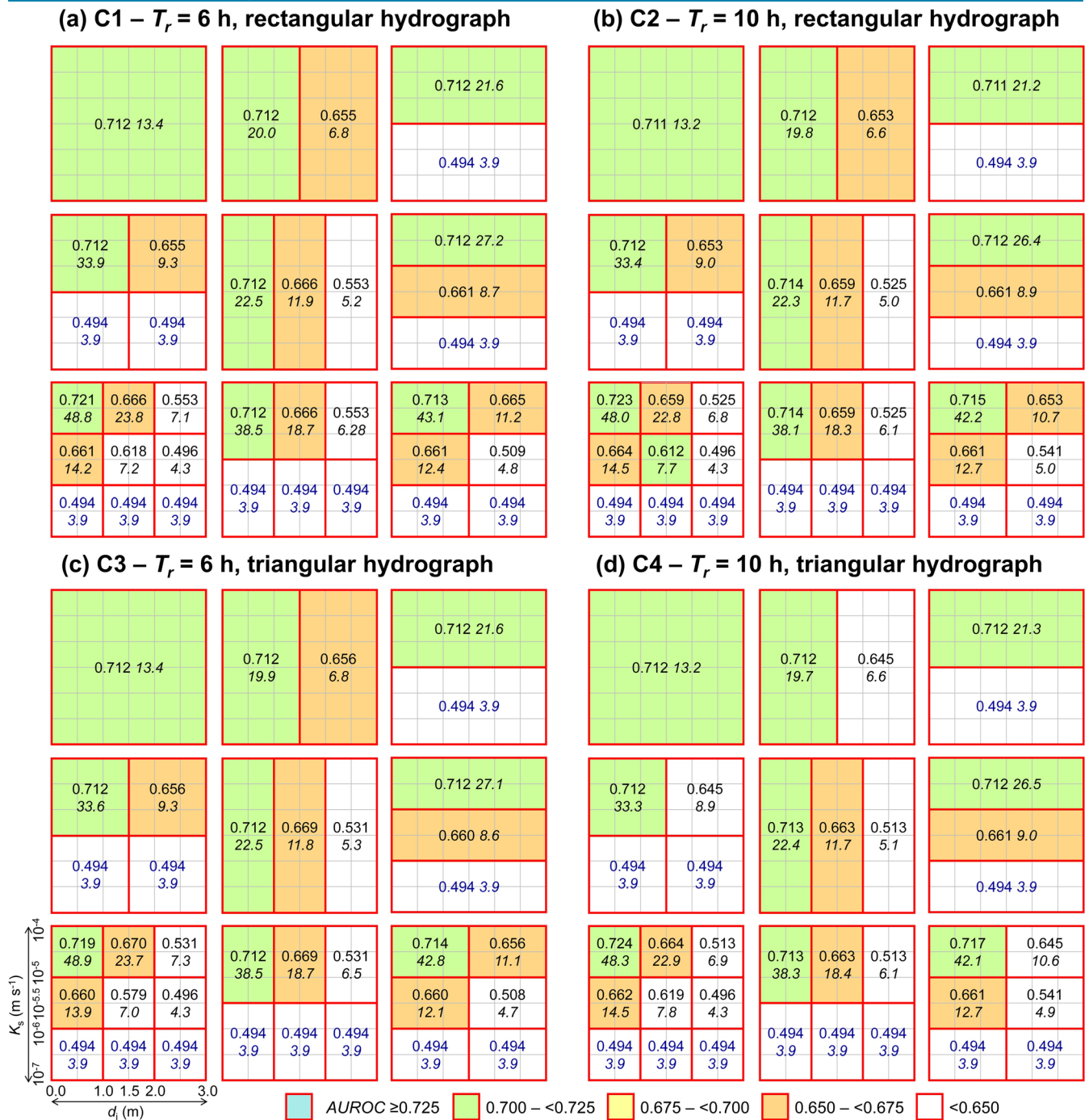


Fig. 7 Results of tests C1–C4 in terms of model performance (AUROC) and factor of conservativeness (FoC, in *italic letters*). See Fig. 3 for the configuration of the parameter space

risk to be off target. The direct effects of the vegetation (not accounted for in the present study) increase the level of uncertainty particularly in forested areas.

The conservativeness of the result in terms of FoC strongly depends on the parameter sub-spaces used as input. μ_{FSI} is generally much higher than r_{OP} indicating that the model results tend to be very conservative. The ideal result should correspond to FoC = 1. Theoretically, this could be achieved by increasing the upper thresholds of the geotechnical parameters, i.e. to make the parameter spaces considered

broader. However, substantially higher parameter thresholds are not realistic for the soil materials involved. We believe that the key for bringing μ_{FSI} in line with r_{OP} consists in appropriately capturing the fine-scale spatial variation of the geotechnical parameters: sliding surfaces most likely coincide spatially with geotechnically susceptible areas, layers or interfaces, spaced in a more or less irregular way. We consider it almost impossible to parameterize such patterns in a deterministic way. In this context, we note that in Figs. 6 and 8, some landslides coincide spatially with areas of low FSI. Such

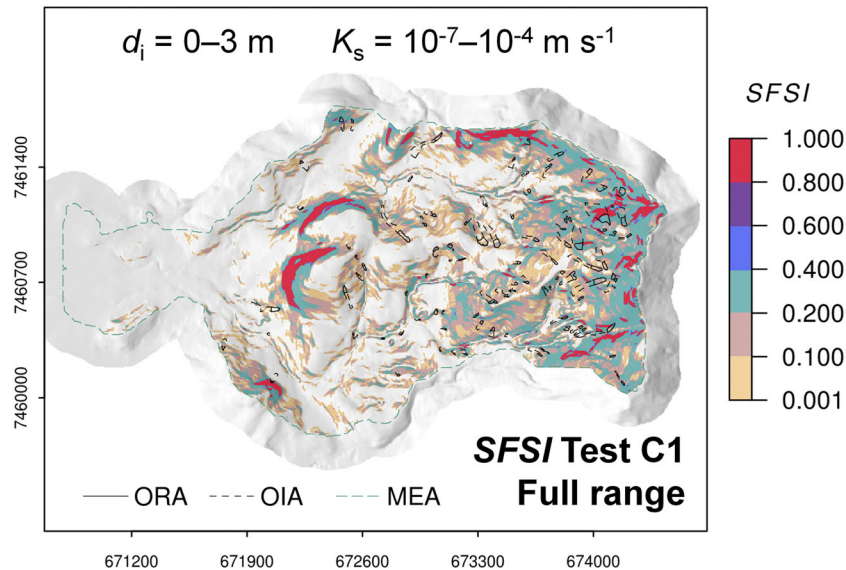


Fig. 8 SFSI map resulting from test C1 with the full parameter range of K_s and d_i . MEA model evaluation area

mispredictions are most probably related to localized patches of low soil strength, increased water input or increased hydraulic conductivity or the effects of the vegetation. Whilst the variation in the local slope angle explains much of the pattern of SFSI, the residual part is most likely explained by fine-scale spatial variations of the soil and, possibly, the vegetation.

Consequently, physically based landslide susceptibility maps can be produced with a minimum amount of geotechnical data but in this case only provide relative results. There is no benefit in dedicating major resources to the detailed investigation of the geotechnical and geohydraulic parameters for catchment-scale landslide susceptibility maps without accounting in detail for the spatial variation of those parameters. Various studies emphasize the major challenges in capturing the spatial variability of the key parameters such as c' and ϕ' (Mergili et al. 2015), K_s (Mesquita et al. 2002, 2007; Mesquita and

Moraes 2004) or soil depth (McBratney et al. 2003; Frohn and Müller 2015). More precisely, at this time, there are no means to appropriately regionalize the key input parameters of slope stability models. We have demonstrated that ad-hoc assumptions of parameter variations (soil depth) may result in a decreased model performance or, in combination with inappropriate reference data (an inventory including transit and deposition areas), may pretend an improved model performance. Notwithstanding any possible future progress in this field, we highlight two strategies to deal with the challenges identified:

1. Accepting the limitations described and interpreting the outcomes of physically based landslide susceptibility models in a relative way. The SFSI as suggested in the present work is one possibility to do so; other ways were introduced earlier with SHALSTAB (Montgomery and Dietrich 1994) or SINMAP (Pack

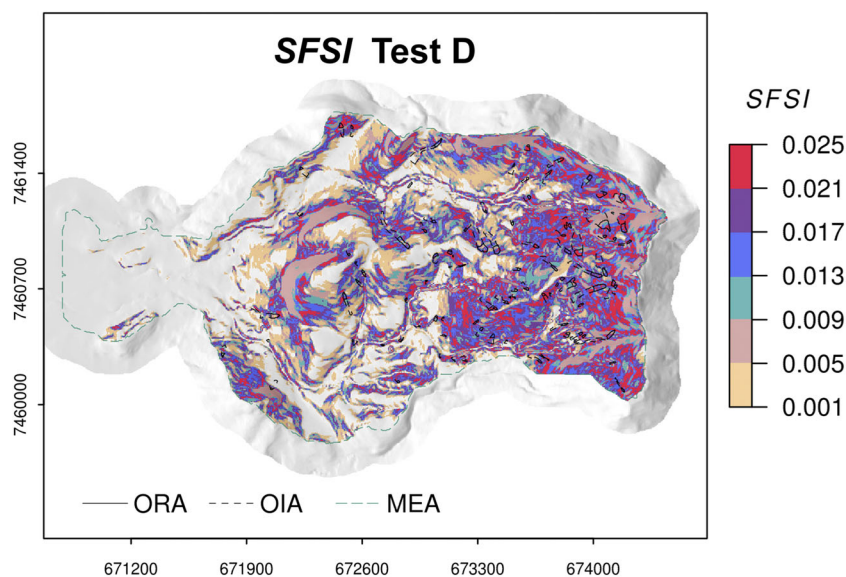


Fig. 9 SFSI map resulting from test D. MEA model evaluation area

et al. 1998). In principle, all slope stability software tools can be used to derive relative indices from multiple results.

2. Using probabilistic approaches to deal with the spatial parameter variation, i.e. resulting in the identification of the possible size of weak regions (Fan et al. 2016). Fibre bundle models may then be used to simulate the associated patterns of slope failures (Cohen et al. 2009). However, this method also relies on various assumptions of spatial parameter variability.

One may argue that also statistical models—employing a black box in terms of relating predictor layers to a landslide inventory—would do the job of producing relative landslide susceptibility maps. In fact, those approaches may be considered a more honest strategy, compared to physically based calculations with uncertain or even unknown geotechnical and geohydraulic parameters. We have shown that even a simplistic statistical model—employing the local slope as the only predictor layer—performs comparable to the more complex physically based models used. This finding reflects the dominant effect of the slope also in the physically based models, as long as the majority of the other key parameters is assumed constant in space. It reminds of the statement of Box (1976) that it would be simple and evocative models pushing science forward rather than over-elaborated, over-parameterized ones. However, it is clear that statistical models would hardly do the work for dynamic analyses such as—with the data usually available—predicting the slope stability response to a particular rainfall event.

Conclusions

We have tested the sensitivity of catchment-scale slope stability model results to variations in the geotechnical and geohydraulic parameters. In contrast to many previous studies, we have focused on parameter spaces instead of combinations of parameter values. The results produced with broad parameter sub-spaces show comparable levels of performance in terms of *AUROC* to those produced with narrow sub-spaces, even though the results vary considerably in terms of *FoC*. In general, the *SFSI* maps are classified as very conservative ($FoC > 1$). It seems obsolete to optimize the parameters tested by means of statistical procedures.

Considering the uncertainty inherent in all geotechnical and geohydraulic data, and the impossibility to capture the spatial distribution of the parameters by means of laboratory tests in sufficient detail, we conclude that landslide susceptibility maps yielded by catchment-scale physically based models should not be interpreted in absolute terms. We suggest that efforts to develop better strategies for dealing with the uncertainties in the spatial variation of the key parameters should be given priority in future slope stability modelling efforts. Even though we consider it likely that many of our results are valid for most types of landslides or geological settings, more tests including a broad spectrum of situations would be necessary to confirm all statements.

Acknowledgements

Open access funding provided by University of Natural Resources and Life Sciences Vienna (BOKU). We are grateful to Prof. Renato Guimarães for kindly providing the DEM and the landslide inventory. Further, we thank National Department of Transportation Infrastructure (DNIT, Brazil) for enabling this work and Capes (Coordination of Higher Education Training, Brazil) for their generous support.

Open Access This article is distributed under the terms of the Creative Commons Attribution 4.0 International License (<http://creativecommons.org/licenses/by/4.0/>), which permits unrestricted use, distribution, and reproduction in any medium, provided you give appropriate credit to the original author(s) and the source, provide a link to the Creative Commons license, and indicate if changes were made.

References

- Baum RL, Savage WZ, Godt JW (2008) TRIGRS—a Fortran program for transient rainfall infiltration and grid-based regional slope-stability analysis, Version 2.0. USGS Open File Report 2008–1159. <https://pubs.usgs.gov/of/2008/1159/downloads/pdf/OF08-1159.pdf>. Accessed 07 December 2015
- Box GE (1976) Science and statistics. *J Am Stat Assoc* 71:791–799. doi:10.2307/2286841
- Burton A, Bathurst JC (1998) Physically based modelling of shallow landslide sediment yield at a catchment scale. *Environ Geol* 35(2):89–99. doi:10.1007/s002540050296
- Carlsaw HS, Jaeger JC (1959) Conduction of heat in solids. Oxford University Press, New York
- Coelho Netto AL (2005) Interface florestal-urbana e os desastres naturais relacionados à água no maciço da Tijuca: desafios ao planejamento urbano numa perspectiva sócio-ambiental. *Revista do Departamento de Geografia* 16:46–60. doi:10.7154/RDG.2005.0016.0005
- Cohen D, Lehmann P, Or D (2009) Fiber bundle model for multiscale modeling of hydromechanical triggering of shallow landslides. *Water Resour Res* 45:W10436. doi:10.1029/2009WR007889
- Conti A (2012) Desenvolvimento de um modelo matemático transiente para previsão de escorregamentos planares em encostas. Dissertation, PUC-Rio
- Duan Q, Sorooshian S, Gupta V (1992) Effective and efficient global optimization for conceptual rainfall-runoff models. *Water Resour Res* 28:1015–1031. doi:10.1029/91WR02985
- Duncan JM, Wright SG (2005) Soil strength and slope stability. Wiley, USA
- Eberhart RC, Kennedy J (1995) A new optimizer using particle swarm theory. In: *Proceedings of the Sixth International Symposium on Micro Machine and Human Science* 1:39–43. doi:10.1109/MHS.1995.494215
- El-Ramly H, Morgenstern NR, Cruden DM (2005) Probabilistic assessment of stability of a cut slope in residual soil. *Géotechnique* 55:77–84. doi:10.1680/geot.2005.55.1.77
- Fan L, Lehmann P, Or D (2016) Effects of soil spatial variability at the hillslope and catchment scales on characteristics of rainfall-induced landslides. *Water Resources Research* 52(3):1781–1799
- Fernandes NF, Guimarães RF, Gomes RAT, Vieira BC, Montgomery DR, Greenberg H (2001) Condicionantes Geomorfológicas dos Deslizamentos nas Encostas: Avaliação de Metodologias e Aplicação de Modelo de Previsão de Áreas Suscetíveis. *Revista Brasileira de Geomorfologia* 2(1):51–71. doi:10.20502/rbg.v2i1.8
- Fischer JT (2013) A novel approach to evaluate and compare computational snow avalanche simulation. *Nat Hazards Earth Syst Sci* 13(6):1655–1667. doi:10.5194/nhess-13-1655-2013
- Formetta G, Capparelli G, Versace P (2015) Evaluating performances of simplified physically based models for landslide susceptibility. *Hydrol Earth Syst Sci Discuss* 12:13217–13256. doi:10.5194/hessd-12-13217-2015
- Frohn D, Müller J (2015) Spatial distribution of clay minerals and soil depth in the Collazzone area, Umbria, central Italy. Master thesis, University of Natural Resources and Life Sciences (BOKU), Vienna
- Galindo MSV (2013) Desenvolvimento de uma Metodologia para Determinação da Viscosidade de Solos. Dissertation, PUC-Rio. doi:10.17771/PUCRio.acad.22977
- Galindo MSV, De Campos TMP (2014) Desenvolvimento de uma Metodologia para Determinação da Viscosidade de Solos. XVII Congresso de Mecânica dos Solos e Engenharia Geotécnica, Goiânia - GO - Brasil
- Godt JW, Baum RL, Savage WZ, Salciarini D, Schulz WH, Harp EL (2008) Transient deterministic shallow landslide modeling: requirements for susceptibility and hazard assessments in a GIS framework. *Eng Geol* 102:214–226. doi:10.1016/j.enggeo.2008.03.019
- GRASS Development Team (2016) Geographic resources analysis support system (GRASS) software. Open Source Geospatial Foundation Project. <http://grass.osgeo.org>. Accessed 11/05/2016
- Griffiths DW, Fenton GA (2004) Probabilistic slope stability analysis by finite elements. *J Geotech Geoenviron* 130(5):507–518. doi:10.1061/(ASCE)1090-0241(2004)130:5(507)
- Griffiths DV, Huang J, Dewolf GF (2011) Numerical and analytical observations on long and infinite slopes. *Int J Numer Anal Methods Geomech* 35(5):569–585. doi:10.1002/nag.909

- Guimarães RF (2000) A modelagem matemática na avaliação de áreas de risco a deslizamentos: o exemplo das bacias dos rios Quitite e Papagaio (RJ). PhD Thesis, Federal University of Rio de Janeiro
- Guimarães RF, Montgomery DR, Greeberg HM, Fernandes NF, Gomes RAT, Carvalho Júnior OA (2003) Parametrization of soil properties for a model of topographic controls on shallow landsliding: application to Rio de Janeiro. *Eng Geol* 69:99–108. doi:10.1016/S0013-7952(02)00263-6
- Guimarães RF, Gomes RAT, Carvalho Júnior OA, Martins ES, Oliveira SN, Fernandes NF (2009) Análise temporal das áreas susceptíveis a escorregamentos rasos no Parque Nacional da Serra dos Órgãos (RJ) a partir de dados pluviométricos. *Revista Brasileira de Geociências* 39(1):190–198. <http://rbg.sbgeo.org.br/index.php/rbg/article/view/1451>. Accessed: 30/11/2015
- Guzzetti F (2006) Landslide hazard and risk assessment. PhD Thesis, University of Bonn
- Guzzetti F, Carrara A, Cardinali M, Reichenbach P (1999) Landslide hazard evaluation: a review of current techniques and their application in a multi-scale study, Central Italy. *Geomorphology* 31:181–216. doi:10.1016/S0169-555X(99)00078-1
- Hay LE, Leavesley GH, Clark MP, Markstrom SL, Viger RJ, Umemoto M (2006) Step wise, multiple objective calibration of a hydrologic model for a snowmelt dominated basin. *J Am Water Resour Assoc*:877–890. doi:10.1111/j.1752-1688.2006.tb04501.x
- Hovland HJ (1977) Three-dimensional slope stability analysis method. *J Geotech Eng Div* 103(9):971–986
- Hurtado Espinoza LO (2010) Avaliação do Potencial de Liquefação de Solos Coluvionares do Rio de Janeiro. Dissertation, PUC-Rio. doi: 10.17771/PUCRio.acad.17520
- Iverson RM (2000) Landslide triggering by rain infiltration. *Water Resour Res* 36(7):897–1910. doi:10.1029/2000WR900090
- Jia N, Mitani Y, Xie M, Djamaluddin I (2012) Shallow landslide hazard assessment using a three-dimensional deterministic model in a mountainous area. *Comput Geotech* 45:1–10. doi:10.1016/j.compgeo.2012.04.007
- McBratney AB, Mendonça Santos ML, Minasny B (2003) On digital soil mapping. *Geoderma* 117:3–52. doi:10.1016/S0016-7061(03)00223-4
- Mergili M, Chu H-J (2015) Integrated statistical modelling of spatial landslide probability. *Nat Hazards Earth Syst Sci Discuss* 3:5677–5715. doi:10.5194/nhessd-3-5677-2015
- Mergili M, Fellin W, Moreiras SM, Stötter J (2012) Simulation of debris flow in the Central Andes based on open source GIS: possibilities, limitations, and parameter sensitivity. *Nat Hazards* 61:1051–1081. doi:10.1007/s11069-011-9965-7
- Mergili M, Marchesini I, Alvioli M, Metz M, Schneider-Muntau B, Rossi M, Guzzetti F (2014a) A strategy for GIS-based 3-D slope stability modelling over large areas. *Geosci Model Dev* 7:2969–2982. doi:10.5194/gmd-7-2969-2014
- Mergili M, Marchesini I, Rossi M, Guzzetti F, Fellin W (2014b) Spatially distributed three-dimensional slope stability modelling in a raster GIS. *Geomorphology* 206:178–195. doi:10.1016/j.geomorph.2013.10.008
- Mergili M, Marchesini I, Rossi M, Alvioli M, Schneider-Muntau B, Cardinali M, Ardizzone F, Fiorucci F, Valigi D, Santangelo M, Bucci F, Guzzetti F (2015) Considering parameter uncertainty in a GIS-based sliding surface model for large areas. In Schweckendiek T, van Tol AF, Pereboom D, van Staveren MT, Cools PMCBM (eds) *Geotechnical Safety and Risk V* (Proceedings of the 5th International Symposium for Geotechnical Safety and Risk (ISGSR2015), Rotterdam, 13–16 October 2015): 952–957. IOS Press. doi: 10.3233/978-1-61499-580-7-952
- Mesquita MGBF, Moraes SOA (2004) Dependência entre a condutividade hidráulica saturada e atributos físicos do solo. *Ciência Rural* 34(3):963–969. doi:10.1590/S0103-84782004000300052
- Mesquita MGBF, Moraes SO, Corrente JE (2002) More adequate probability distributions to represent the saturated soil hydraulic conductivity. *Sci Agric* 59(4):789–793. doi:10.1590/S0103-90162002000400025
- Mesquita MGBF, Moraes SO, Peruchi F, Tereza MC (2007) Alternativa para caracterização da condutividade Hidráulica saturada do solo utilizando probabilidade de ocorrência. *Ciência Agrotécnica* 31(6):1605–1609. doi:10.1590/S1413-70542007000600001
- Milledge DG, Griffiths DV, Lane SN, Warburton J (2012) Limits on the validity of infinite length assumptions for modelling shallow landslides. *Earth Surface Process and Landforms* 37:1158–1166. doi:10.1002/esp.3235
- Miquelotto M, Vargas Jr. EA (2009) Avaliação tridimensional da estabilidade de encostas em escala de bacia de drenagem através do método de talude infinito incorporando o efeito do fluxo saturado-não saturado. *Anais da 5ª Conferencia de Estabilidade de Encosta*, São Paulo, SP, Brasil
- Montgomery DR, Dietrich WE (1994) A physically based model for the topographic control on shallow landsliding. *Water Resour Res* 30:1153–1171. doi:10.1029/93WR02979
- Moore ID, Grayson RB, Ladson AR (1991) Digital terrain modeling—a review of hydrological, geomorphological, and biological applications. *Hydrol Process* 5:3–30. doi:10.1002/hyp.3360050103
- Muntohar AS, Liao H-J (2010) Rainfall infiltration: infinite slope model for landslides triggering by rainstorm. *Nat Hazards* 54:967–984. doi:10.1007/s11069-010-9518-5
- Neteler M, Mitasova H (2008) Open source GIS: a GRASS GIS approach. Springer, New York. doi:10.1007/978-0-387-68574-8
- Pack RT, Tarboton DG, Goodwin CN (1998) The SINMAP approach to terrain stability mapping. 8th Congress of the International Association of Engineering Geology, Vancouver, BC. doi: 10.1.1.41.5799
- Park DW, Nikhil NV, Lee SR (2013) Landslide and debris flow susceptibility zonation using TRIGRS for the 2011 Seoul landslide event. *Natural Hazards Earth System Sciences* 13:2833–2849. doi:10.5194/nhess-13-2833-2013
- Petrovic I (2008) Probabilistic stability analysis of sanitary landfill Jakusevec. *Proceedings of the 1st Middle European Conference on Landfill Technology*, Budapest, Hungary
- R Core Team (2016) R: a language and environment for statistical computing, R foundation for statistical computing. <https://cran.r-project.org/doc/manuals/r-release/fullrefman.pdf>. Accessed: 11/05/2016
- Saltelli A, Annoni P (2010) How to avoid a perfunctory sensitivity analysis. *Environmental Modelling and Software* 25:1508–1517. doi:10.1016/j.envsoft.2010.04.012
- Saxton KE, Rawls WJ (2006) Soil water characteristic estimates by texture and organic matter for hydrologic solutions. *Soil Science Society of American Journal* 70:1569–1578. doi:10.2136/sssaj2005.0117
- Tobutt DC (1982) Monte Carlo simulation methods for slope stability. *Comput Geosci* 8(2):199–208. doi:10.1016/0098-3004(82)90021-8
- Van Westen CJ (2000) The modelling of landslide hazards using GIS. *Surveys Geophysics* 21:241–255. doi:10.1023/A:1006794127521
- Van Westen CJ, Terlien MTJ (1996) An approach towards deterministic landslide hazard analysis in GIS: a case study from Manizales (Colombia). *Earth Surface Processes Landforms* 21:853–868. doi:10.1002/(SICI)1096-9837(199609)21:9<853::AID-ESP676>3.0.CO;2-C
- VanWesten CJ, Van Asch TWJ, Soeters R (2006) Landslide hazard and risk zonation—why is it still so difficult? *Bull Eng Geol Environ* 65:167–184. doi:10.1007/s10064-005-0023-0
- Vrugt JA, ter Braak CJF, Clark MP, Hyman JM, Robinson BA (2008) Treatment of input uncertainty in hydrologic modeling: doing hydrology backward with Markov chain Monte Carlo simulation. *Water Resour Res* 44:W00B09. doi:10.1029/2007WR006720, 2
- Wang Y, Cao Z, Au SK (2010) Practical reliability analysis of slope stability by advanced Monte Carlo simulations in spreadsheet. *Can Geotech J* 48(1):162–172. doi:10.1139/T10-044
- Wilkinson PL, Anderson MG, Lloyd DM (2002) An integrated hydrological model for slope stability. *Earth Surface Processes Landform* 27:1267–1283. doi:10.1002/esp.409
- Xie M, Zhou G, Mitani Y (2003) Three-dimensional stability evaluation of landslides and a sliding process simulation using a new geographic information systems component. *Environ Geol* 43:503–512. doi:10.1007/s00254-002-0655-3
- Xie M, Esaki T, Cai M (2004a) A time-space based approach for mapping rainfall induced shallow landslide hazard. *Environ Geol* 46:840–850. doi:10.1007/s00254-004-1069-1
- Xie M, Esaki T, Cai M (2004b) A GIS-based method for locating the critical 3D slip surface in a slope. *Comput Geotech* 31:267–277. doi:10.1016/j.compgeo.2004.03.003
- Xie M, Esaki T, Qiu C, Wang C (2006) Geographical information system-based computational implementation and application of spatial three-dimensional slope stability analysis. *Comput Geotech* 33:260–274. doi:10.1016/j.compgeo.2006.07.003

C. de Lima Neves Seefelder

National Department of Transportation Infrastructure (DNIT),
Setor de Autarquias Norte, Quadra 03 Lote A, Ed. Núcleo dos Transportes, Brasília – DF, 70.040-902, Brazil

C. de Lima Neves Seefelder · S. Koide

Department of Civil Engineering,
University of Brasília,
Anexo SG-12 – Térreo, Campus Universitário Darcy Ribeiro, Brasília – DF, 70.910-900, Brazil

C. de Lima Neves Seefelder · M. Mergili

Geomorphological Systems and Risk Research, Department of Geography and Regional Research,
University of Vienna,
Universitätsstraße 7, 1190, Vienna, Austria

M. Mergili

Institute of Applied Geology,
University of Natural Resources and Life Sciences (BOKU),
Peter-Jordan-Straße 70, 1190, Vienna, Austria